ENHANCED ATTITUDE CONTROL EXPERIMENT FOR SSTI LEWIS SPACECRAFT

Peiman G. Maghami

NASA Langley Research Center
Mail Stop 161
Hampton, Virginia 23681–0001

Abstract

The enhanced attitude control system experiment is a technology demonstration experiment on the NASA's small spacecraft technology initiative program's Lewis spacecraft to evaluate advanced attitude control strategies. The purpose of the enhanced attitude control system experiment is to evaluate the feasibility of designing and implementing robust multi-input/multi-output attitude control strategies for enhanced pointing performance of spacecraft to improve the quality of the measurements of the science instruments. Different control design strategies based on modern and robust control theories are being considered for the enhanced attitude control system experiment. This paper describes the experiment as well as the design and synthesis of a mixed H_2/H_∞ controller for attitude control. The control synthesis uses a nonlinear programming technique to tune the controller parameters and impose robustness and performance constraints. Simulations are carried out to demonstrate the feasibility of the proposed attitude control design strategy.

Introduction

The current practice in spacecraft attitude control design is based on a single-input/single-output (SISO) control strategy, wherein elementary and low bandwidth controllers are designed for each of the three-axes of the spacecraft separately. Typically, SISO attitude controllers are designed to be low bandwidth (gain stabilized) to avoid uncertain, and possibly harmful, interactions with the flexible modes of the spacecraft, such as those of solar arrays or antennas [1–2]. However, these controllers have limited performance because of their elementary structure and low bandwidth. Moreover, they are fairly hard to modify in their flight software implementation form because they are typically coded to follow a specific controller order and type. The enhanced attitude control system (EACS) experiment is a technology demonstration experiment on the NASA's small spacecraft technology initiative (SSTI) program's Lewis spacecraft to evaluate advanced attitude control strategies. The purpose of the EACS experiment is to evaluate the feasibility of designing and implementing robust multi-input/multi-output (MIMO) attitude control strategies for enhanced pointing performance of spacecraft to improve the quality of the measurements of the science instruments. This experiment is limited to controller designs for attitude control in the normal science mode which involves fine attitude pointing. The MIMO control designs would utilize robust and modern control theories to synthesize attitude control designs which can take better advantage of the control system hardware to provide higher authority controllers, i.e., phase or gain stabilized. Moreover, once an algorithm is incorporated on the spacecraft to implement a MIMO attitude control system (ACS) design, it would be very easy to replace controllers. The specific objectives of the experiment are as follows:

1. To develop a MIMO ACS algorithm and flight software, and implement this software within the SSTI/Lewis flight on-board computer software
2. To develop MIMO attitude control designs, based on robust and modern control theory
3. To conduct attitude control experiments by implementing the MIMO control designs (instead of the baseline normal mode controller) in the normal pointing mode
4. To evaluate the performance of MIMO attitude control designs by analyzing the telemetry data

An efficient algorithm, both in time and memory requirements, for the implementation of MIMO controllers has been developed. With this algorithm, the required memory and the number of floating point operations are linear functions of the number of states in the MIMO controller. The implementation software has been developed and incorporated within the on-board flight computer software. The enhanced attitude control system is implemented as an independent module within the ACS software. It should be noted that the various MIMO control designs are implemented by simply uploading the controller data sets into the MIMO routine, which also indicates the ease of replacing the controller with a new MIMO control design. Several synthesis techniques are being considered for the design of MIMO controllers for the EACS experiment. These include, H_2–based, H_∞–based, μ–based designs, as well as others. One of the techniques considered is a mixed H_2/H_∞ control synthesis approach, which is described in this paper. In this control synthesis approach, a nonlinear programming technique is used to tune the controller parameters of an H_2–based controller while imposing H_∞–based robustness constraints, as well as, additional performance constraints. The MIMO controllers are applied to a model of the Lewis spacecraft, and simulations are carried out to demonstrate the feasibility of the proposed attitude control design strategy.

Spacecraft Modeling

For the purpose of dynamics and control design and analysis, the task of modeling a spacecraft can be divided into the modeling of the spacecraft structure itself, and the modeling of the actuator components, sensor components, and the controller, all of which comprise the attitude control system.

Spacecraft structure modeling

Typically, the spacecraft structure can be modeled as a linear, time-invariant flexible system, which in turn can be represented by the following second-order dynamical equations:

$$M\ddot{x} + D\dot{x} + Kx = Bu + Hv \tag{1}$$

together with some set of measurement and performance output equations:

$$\begin{aligned} y_d &= C_{md}x, \quad y_{\mathrm{v}} = C_{m\mathrm{v}}\dot{x} \\ y_{pd} &= C_{pd}x, \quad y_{p\mathrm{v}} = C_{p\mathrm{v}}\dot{x} \end{aligned} \tag{2}$$

where M is the positive definite mass matrix; D is the positive semidefinite damping matrix; K is the positive semidefinite stiffness matrix; B is the input influence matrix; H is the disturbance input influence matrix; C_{md} and $C_{m\mathrm{v}}$ are the attitude and attitude rate measurement output influence matrices, respectively; C_{pd} and $C_{p\mathrm{v}}$ are attitude and attitude rate performance output influence matrices, respectively; x is a k x 1 vector of displacements; u is a m x 1 vector of inputs to the system; v is a e x 1 vector of disturbances to the system; y_d and y_{v} are the attitude and attitude rate measurement output vectors, respectively; and y_{pd} and y_{pv} are the attitude and attitude rate performance output vectors, respectively. Usually, a finite element analysis is used to obtain these matrices. In most cases, the number of displacements, k, is quite large and thus impractical to work with for general design and analysis purposes. To make the problem more tractable, the displacements vector x is transformed into modal coordinates using the transformation $x = \Phi r$, with r being a n x 1 vector of modal amplitudes and n << k. Here, only n significant modes are retained. The transformation matrix Φ contains n columns which are the eigenvectors associated with the n modes of interest of the flexible system. The equations for the system, in transformed coordinates, are:

$$\begin{aligned} M_r\ddot{r} + D_r\dot{r} + K_r r &= \Phi^T B u + \Phi^T H v \\ y_d = C_{md}\Phi r,\ y_{\mathrm{v}} &= C_{m\mathrm{v}}\Phi\dot{r} \\ y_{pd} = C_{pd}\Phi r,\ y_{pv} &= C_{p\mathrm{v}}\Phi\dot{r} \end{aligned} \tag{3}$$

If normal modes are used, and their mode shapes have been normalized with respect to the mass matrix, and modal damping is assumed, then $M_r = I_{nxn}$, $K_r = diag\left(\omega_1^2, \omega_2^2, ..., \omega_n^2\right)$ and $D_r = diag(2\zeta_1\omega_1, 2\zeta_2\omega_2, ..., 2\zeta_n\omega_n)$, with w_i and ζ_i being the open-loop natural frequency and damping ratio values, respectively, for the ith mode.

By defining a new vector $x_s = [r^T \quad \dot{r}^T]^T$, the second-order equations in eq. (3) can be rewritten into first-order form as:

$$\begin{aligned} \dot{x}_s &= A_s x_s + B_s u + B_d v \\ A_s &= \begin{bmatrix} 0 & I_{n\mathrm{x}n} \\ -K_r & -D_r \end{bmatrix}; \\ B_s &= \begin{bmatrix} 0 \\ \Phi^T B \end{bmatrix};\ B_d = \begin{bmatrix} 0 \\ \Phi^T H \end{bmatrix} \end{aligned} \tag{4}$$

The measurement and performance output equations can then be written as:

$$\begin{aligned} y &= \begin{bmatrix} y_d \\ \\ y_v \end{bmatrix} = Cx_s \\ y_p &= \begin{bmatrix} y_{pd} \\ \\ y_{p\mathrm{v}} \end{bmatrix} = C_p x_s \\ C &= \begin{bmatrix} C_{md}\Phi & 0 \\ \\ 0 & C_{mv}\Phi \end{bmatrix}; \\ C_p &= \begin{bmatrix} C_{pd}\Phi & 0 \\ \\ 0 & C_{p\mathrm{v}}\Phi \end{bmatrix}; \end{aligned} \tag{5}$$

Here, x_s is the plant state vector; A_s is the plant state matrix; B_s is the control input influence matrix; C and C_p denote the measurement output and performance output influence matrices, respectively.

Attitude Control System Modeling

In addition to modeling the spacecraft structure, or plant, the various components of the attitude control system (ACS) should be included to complete the spacecraft model. These components are the sensors, actuators and computer/data acquisition systems required to control the spacecraft. By including these components, significant real world effects such as actuator and sensor dynamics, noise, digital quantization and sampling time delays, can be accounted for in the overall analysis model. A typical ACS, depicted in block diagram form with the plant in the loop, is shown in Figure 1.

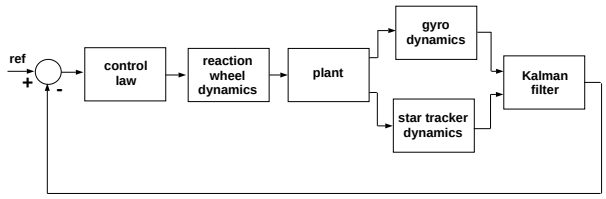

Figure 1. Typical ACS model components.

This block diagram represents a typical ACS simulation model for a spacecraft. The ACS consists of reaction wheels to provide the attitude maneuvering and control torques, with rate gyros and a star tracker, as sensors for measuring the spacecraft attitudes and attitude rates. The Kalman filter is used to estimate the vehicle's attitude from the sensor data, and the control law uses these estimated values, together with the attitude rate measurements from the gyros, to compute the appropriate torque commands. The reaction wheel dynamics may include nonlinear effects, like friction and stiction, limits on the input command voltages and digital voltage quantization, as well as the quantization effects on wheel RPM outputs due to the wheel's optical encoder. Each rate gyro senses the spacecraft attitude rates in one axis, and is modeled as a second-order system. Rate gyro units may be combined to comprise multi-axis gyro packages. To each gyro dynamic model output channel, random signals are added, which represent random drift walk and instrument noise. The modeling of the star tracker may include noise and alignment errors. Digital computer effects are modeled by performing the control law and Kalman filtering computations in discrete form, and using the appropriate sampling times for each.

The equations governing the dynamics of the ACS components are generally nonlinear, however, for the purpose of MIMO control designs a linear model which includes a linearized model of the wheel speed controller dynamics, a 2nd-order Pade approximation of a unit time delay of 1.024 sec (wheel speed controller time cycle), and a rational approximation of a zero-order hold at 1.024 sec, is used to represents the control system dynamics. These dynamics can be written in the form

$$\begin{aligned} \dot{x}_h &= A_h x_h + B_h \overline{u} \\ u &= C_h x_h + D_h \overline{u} \end{aligned} \tag{6}$$

where x_h is a vector of states for the ACS components; A_h, B_h, C_h, and D_h are the corresponding system matrices; and $\overline{u}$ is the vector of commanded control inputs. These equations can then be combined with the spacecraft dynamics equations in eqs. 4 and 5 to form the complete set of spacecraft system equations.

Control Synthesis

As mentioned earlier, several synthesis techniques are being considered in the EACS experiment for the design of MIMO controllers. These include, H_2–based, H_∞–based, μ–based, and other controllers. One technique considered is a mixed H_2/H_∞ approach, implemented through design optimization, which is described in this paper. In this approach, the controller is synthesized following H_2 methods while robustness constraints, to guarantee robustness against model uncertainties in the plant, input, and output, are imposed through H_∞–type constraints. The H_2 design follows the LQG/LTR (Loop Transfer Recovery) methodology to provide stabilizing controllers for the enhanced attitude control experiment. Loop shaping filters are implemented within the LQG/LTR framework to provide the ability to manipulate the loop gains. The design parameters include the characteristics of the process and measurement noise as well as the variables associated with the shaping filters. At the top level of this synthesis technique, nonlinear programming is used to optimize the design parameters to provide optimal pointing performance for the Lewis spacecraft while imposing H_∞–type robustness constraints, loop shaping constraints, as well as other design constraints. The details of the synthesis procedure is provided in the following sections.

LQG/LTR

In the LQG/LTR synthesis, the plant is assumed to have the form

$$\begin{aligned} \dot{x} &= Ax + Bu + \Gamma w \\ y &= Cx + v \end{aligned} \tag{7}$$

where x represents the augmented plant state vector defined as $x = \left[x_s^T, x_h^T\right]^T$, which is obtained by combining the spacecraft plant dynamics, given by eqs. (4) and (5), with the control system hardware dynamics, given by eq. (6), in series. The matrices A, B, and C are the augmented spacecraft state, input influence, and output influence matrices, respectively. The vectors w and v are the process and measurement noise vectors, respectively, and are modeled as zero-mean and uncorrelated white noises with covariances

$$E\left\{ww^T\right\} = W \geq 0\,;\; E\left\{vv^T\right\} = V > 0 \tag{8}$$

The optimal LQG controller is given by [3]

$$\begin{aligned} \dot{\hat{x}} &= (A - K_f - BK_c)\hat{x} + K_f y \\ u &= -K_c \hat{x} \end{aligned} \tag{9}$$

with

$$K_c = -R^{-1}B^T P_c\,;\; K_f = P_f C^T V^{-1} \tag{10}$$

where P_f and P_c are positive semidefinite matrices that satisfy the following algebraic Riccati equations.

$$\begin{aligned} A^T P_c + P_c A - P_c B R^{-1} B^T P_c + C^T Q C = 0 \\ P_f A^T + A P_f - P_f C^T V^{-1} C P_f + \Gamma^T W \Gamma = 0 \end{aligned} \tag{11}$$

If the triples $(A,\ B,\ Q^{1/2}C)$ and $(A,\ \Gamma W^{1/2},\ C)$ are stabilizable and detectable, positive semidefinite solutions to the Riccati equations in eq. (11) exist and the resulting controller is stabilizing, i.e., the closed-loop system is stable [3]. Loop transfer recovery is a way of designing the LQG controller such that the desirable robustness and performance characteristics of the full state feedback are recovered at the plant input or output. For a square plant, a two step procedure is followed to achieve LTR at the plant output [3].

1. Design a Kalman filter by choosing appropriate covariance matrices W and V until the return ratio of the filter $-C(sI-A)^{-1}K_f$ is satisfactory for the plant output.
2. Design an optimal regulator by setting $Q = I$ and $R = \rho I$, and choose a ρ small enough such that the return ratio of the compensated plant at the output resembles the return ratio of the filter $-C(sI-A)^{-1}K_f$ with reasonable accuracy over a desired range of frequencies.

It should be noted that in LQG/LTR the noise covariance matrices are taken as design parameters in order to shape the loop gain of the system, and they do not necessarily have any association with process or measurement noise characteristics. In practical applications, the degree of freedom provided by the element of the covariance matrices may not be sufficient to obtain a desired loop gain in particular ranges of frequency. In order to provide additional capability to adjust the loop gain, the spectral distribution of the process and measurement noises may be manipulated in desired frequency regions by augmenting the plant dynamics with additional noise dynamics. For the purpose of MIMO ACS designs for the Lewis spacecraft, the spectral distribution of both the process and measurement noises are manipulated. The spectral distribution of the process noise is manipulated to provide integral action in the loop gain which is critical for acceptable pointing performance. This is achieved by introducing the following dynamics

$$\begin{aligned} \dot{\eta} &= A_w\,\eta + B_w\,\bar{w} \\ w &= C_w\,\eta \end{aligned} \tag{12}$$

with $A_w = -0.0001\alpha$, $B_w = I_{3\times3}$, and $C_w = I_{3\times3}$. Here, $\bar{w}$ is a white noise with intensity W, and α is a 3x3 diagonal matrix, with positive elements that can be adjusted by the design process.

In order to ensure proper roll-off of the loop gain at the higher frequency ranges, to avoid destabilizing spill-over problems or high frequency noise pollution, the spectral distribution of the measurement noise is manipulated by introducing additional dynamics as follows.

$$\begin{aligned} \dot{\xi} &= A_v\,\xi + B_v\,\bar{v} \\ v &= C_v\,\xi + D_v\,\bar{v} \end{aligned} \tag{13}$$

with $A_v = -0.5\beta$, $B_v = I_{3\times3}$, $C_v = -12.5\beta\theta$, and $D_v = 25\theta$. Here, $\bar{v}$ is a white noise with intensity V, and β and θ are 3x3 diagonal matrices, with positive elements that can be adjusted by the design process to shape the roll-off.

The overall system dynamics may be written by combining eqs. (7), (12), and (13), to obtain

$$\begin{aligned} \dot{\bar{x}} &= \bar{A}\bar{x} + \bar{B}u + \bar{\Gamma}\bar{\psi} \\ y &= \bar{C}\bar{x} + \Upsilon\bar{v} \end{aligned} \tag{14}$$

where

$$\begin{gathered} \bar{A} = \begin{bmatrix} A & \Gamma C_w & 0 \\ 0 & A_w & 0 \\ 0 & 0 & A_v \end{bmatrix}; \\ \bar{B} = \begin{bmatrix} B \\ 0 \\ 0 \end{bmatrix};\ \bar{\Gamma} = \begin{bmatrix} 0 & 0 \\ B_w & 0 \\ 0 & B_v \end{bmatrix}; \\ \bar{C} = [C \quad 0 \quad CC_v\,];\ \Upsilon = CD_v \end{gathered} \tag{15}$$

and

$$\psi \equiv \begin{Bmatrix} \bar{w} \\ \bar{v} \end{Bmatrix} \tag{16}$$

with

$$E\left(\psi\psi^T\right) = \Psi = \begin{bmatrix} W & 0 \\ 0 & V \end{bmatrix} \tag{17}$$

Now, the LQG/LTR based attitude control design is synthesized by using variables $\bar{A},\ \bar{B},\ \bar{C},\ \bar{\Gamma},\ \Psi,$ and $\Upsilon V \Upsilon^T$, from eqs. (15) to (17), as $A,\ B,\ C,\ \Gamma,\ W,$ and V, respectively, in eqs. (9) to (11), with $Q = I$, and $\rho = 10^{-8}$. Note that the design freedom is contained in the elements of the covariance matrices W and V, as well as the diagonal elements of matrices $\alpha,\ \beta,$ and θ, i.e., a new controller is synthesized for every combination of these parameters. As mentioned earlier, design optimization is used to choose these parameters so as to optimize the pointing performance of the spacecraft while satisfying robustness and performance constraints.

Robustness

The LQG/LTR controller can provide excellent performance if the model of the system is accurately known. However, this controller may have serious stability and performance issues if there is considerable uncertainty in the model. In typical spacecraft design, the issue of model uncertainty for the SISO controller is treated in the classical sense by imposing stability margins, such as gain and phase margins. In this paper, robust stability for the MIMO ACS controllers is addressed through the application of robust stability theory for various forms of uncertainty in the system model. Specifically, four types of uncertainties are considered, and they are (a) input multiplicative to accommodate uncertainties in the input of the plant, such as the reaction wheels; (b) output multiplicative to accommodate uncertainties in the output of the plant, such as the attitude measurement system; (c) additive to accommodate unmodelled high frequency spacecraft dynamics; and (d) parametric uncertainties to accommodate uncertainties in the modal

frequencies of some of the flexible modes that are included in the design model. The conditions for robust stability of the system under these type of uncertainties is discussed in the following.

Uncertainties in the input

The uncertainties in the actuation system, such as those of the reaction wheel assembly or the controller, as well as general uncertainties in the spacecraft plant model, may be modeled as input multiplicative uncertainty, Δ_i, shown in Figure 2.

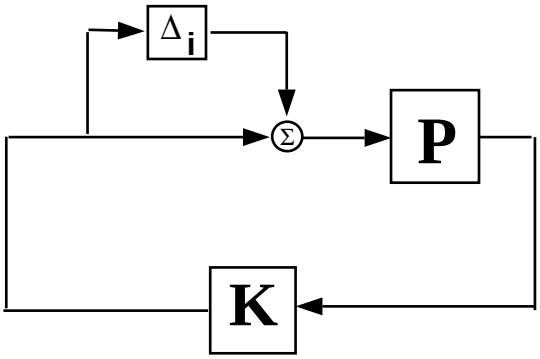

Figure 2. System with Input Multiplicative Uncertainty.

which is equivalent to

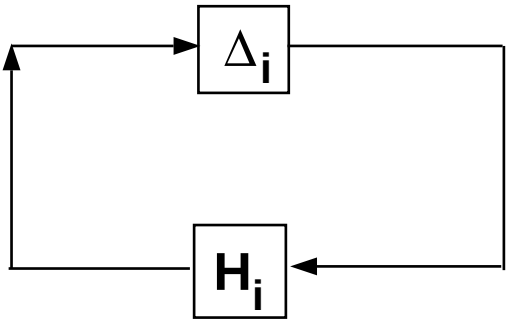

Figure 3. Equivalent System with Input Multiplicative Uncertainty.

where $H_i = (I + KP)^{-1}KP$, with P representing the plant (system in eq. (7) and K denoting the controller (system in eqs. (9) to (11)). The condition for robust stability of the feedback system shown in Figure 3 is established from the small gain theorem [3], which states that the closed-loop system is stable iff

$$\|\Delta_i(jw)\|_\infty < \frac{1}{\|H_i(jw)\|_\infty} \tag{18}$$

From eq. (18), if it is required to allow an input multiplicative uncertainty $\Delta_i(jw)$ such that $\|\Delta_i(jw)\|_\infty \leq \delta_i$, the condition for robust stability can then be written as

$$\|H_i(jw)\|_\infty < \frac{1}{\delta_i} \tag{19}$$

Uncertainties in the Output

The uncertainties in the attitude measurement system, such as those in the rate gyros, star trackers, etc., as well as general uncertainties in the spacecraft plant model, may be modeled as output multiplicative uncertainty, Δ_o, shown in Figure 4.

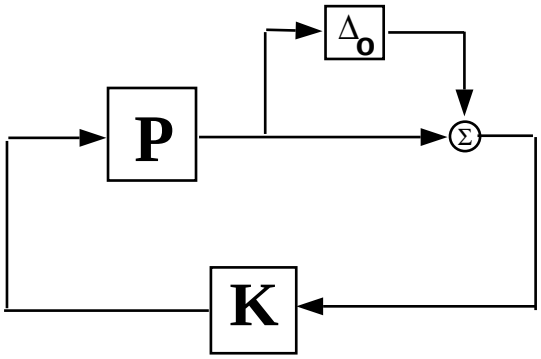

Figure 4. System with Output Multiplicative Uncertainty.

which is equivalent to

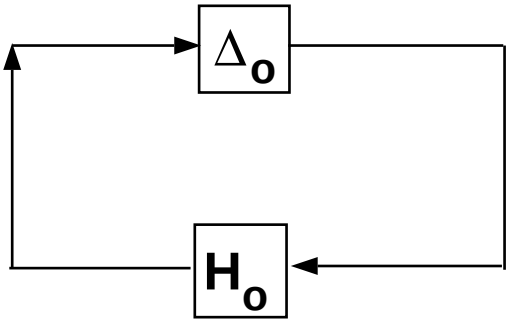

Figure 5. Equivalent System with Output Multiplicative Uncertainty.

where $H_o = (I + PK)^{-1}PK$. The condition for robust stability of the feedback system shown in Figure 5 is established from the small gain theorem [3], which states that the closed-loop system is stable iff

$$\|\Delta_o(jw)\|_\infty < \frac{1}{\|H_o(jw)\|_\infty} \tag{20}$$

From eq. (20), if it is required to allow an output multiplicative uncertainty $\Delta_o(jw)$ such that $\|\Delta_o(jw)\|_\infty \leq \delta_o$, the condition for robust stability can then be written as

$$\|H_o(jw)\|_\infty < \frac{1}{\delta_o} \tag{21}$$

Unmodeled Dynamics

As mentioned earlier, the spacecraft structural model may include hundreds or thousands of flexible modes. However, realistically only a few significant low frequency modes are included in the control design model, i.e., the higher frequency modes are neglected. Moreover, the degree of uncertainty in the knowledge of the frequency and other modal attributes of the flexible modes increase as frequency increases. One option could be to neglect the higher frequency modes, but this could cause performance degradation and even instabilities in the form of spill over. The approach taken here is to model the neglected flexible dynamics along with associated uncertainties as additive plant uncertainty, Δ_a, as shown in Figure 6.

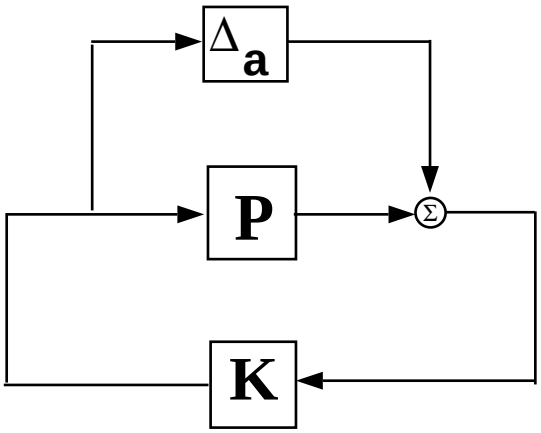

Figure 6. System with Additive Uncertainty.

which is equivalent to

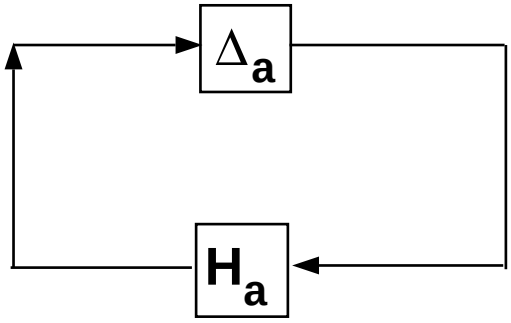

Figure 7. Equivalent System with Additive Uncertainty.

where $H_a = (I + KP)^{-1}K$. Let $\Delta_a(jw)$ be a stable, rational transfer function. Then, the condition for robust stability of the feedback system shown in Figure 7 is established from the small gain theorem [3], which states that the closed-loop system is stable iff

$$\|\Delta_a(jw)\|_\infty < \frac{1}{\|H_a(jw)\|_\infty} \tag{22}$$

Let the unmodeled dynamics along with associated uncertainties be such that the additive uncertainty $\Delta_a(jw)$ is bounded as follows

$$\bar{\sigma}(\Delta_a(jw)) \leq |\delta_a(jw)| \; ; \; \forall\omega \tag{23}$$

where $\delta_a(jw)$ is a scalar, rational, and stable transfer function. The condition for robust stability can then be rewritten as

$$\|\delta_a(jw)H_a(jw)\|_\infty < 1 \tag{24}$$

Uncertainty in modal frequencies

For the purpose of control design, only the first three flexible modes are included in the design model. This is chiefly due to the sampling rate of the control system, which limits the control authority over the flexible modes considerably. Nevertheless, because of uncertainties that may exist in the knowledge of the frequencies of these three modes (parametric uncertainties), it is desirable to design a MIMO ACS controller which provides robust stability in the presence of such uncertainties, i.e., the closed-loop system can tolerate a certain degree of uncertainty in these frequencies. In this paper, robust stability for uncertainties in the frequency of the first two flexible modes, which are most likely to have interactions with the ACS, is considered. Note that uncertainties in the mode shapes or modal damping ratios are not considered because they are not deemed as critical. The parametric uncertainties , Δ_m (see eq. (26), are modeled in a feedback configuration with an augmented plant as shown in Figure 8.

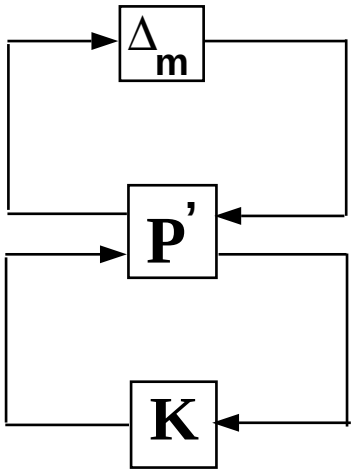

Figure 8. System with Parametric Uncertainty

Here $P^{'}$ represents an augmented plant with additional inputs and outputs to accommodate the two model frequency uncertainties (see eq. (27)). The configuration in figure 8

is equivalent to

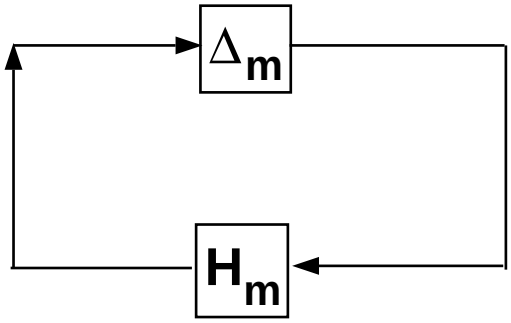

Figure 9. Equivalent System with Parametric Uncertainty

where

$$H_m = \hat{C}(sI - A_{cl})^{-1}\hat{B} \tag{25}$$

and

$$\Delta_m = \begin{bmatrix} \delta_{m1} & 0 \\ 0 & \delta_{m2} \end{bmatrix} \; ; \; \delta_{mi} \in \mathcal{C} \tag{26}$$

Here H_m represents the closed-loop transfer function around the parametric uncertainty. A_{cl} denotes the closed-loop state matrix; and

$$\hat{B} = \begin{bmatrix} 0 & 0 \\ \vdots & \vdots \\ 0 & 0 \\ 1 & 0 \\ 0 & 1 \\ \vdots & 0 \\ \vdots & \vdots \\ 0 & 0 \end{bmatrix} ; \; \hat{C} = \begin{bmatrix} 0 & \dots & 0 & -\omega_1^2 & 0 & \dots & \dots & 0 \\ 0 & \dots & 0 & 0 & -\omega_2^2 & 0 & \dots & 0 \end{bmatrix} \tag{27}$$

Note that the non-zero elements in $\hat{B}$ and $\hat{C}$ correspond to the state variables associated with the modal velocities and displacements of the first two flexible modes, respectively. The condition for robust stability of the feedback system shown in Figures 8 or 9 is given by Doyle [4], and may be stated as follows. The feedback system shown in Figure 9 is stable for Δ_m, $\|\Delta_m\|_\infty < \delta_m$, iff

$$\mu(H_m(jw)) < \frac{1}{\delta_m} \; ; \; \forall\omega \tag{28}$$

or

$$\|H_m(jw)\|_\mu < \frac{1}{\delta_m} \tag{29}$$

Since μ can not be directly computed, i.e., it is typically obtained by bounding it from above and below over a range of frequencies, direct implementation of the robustness condition given in eqs. (28) or (29) is costly and impractical in an optimization setting. Therefore, the condition in eqs. (28) or (29) is replaced by

$$\|H_m(jw)\|_\infty < \frac{1}{\delta_m} \tag{30}$$

Although, this condition is an upper bound for $\mu(H_m)$, and consequently may be more conservative than the previous one, it is computationally more tractable. Furthermore, since the modes are spatially independent (corresponding to two different principal axes of the spacecraft), and the plant and the controller tend to be diagonally dominant in this frequency range, it is expected that the condition in eq. (30) would not be too conservative. However, in actuality no matter what condition for robust stability is used (eqs. (28), (29), (30)), since the control authority over these two modes is fairly limited, the condition for robust stability tends to be conservative, i.e., $\delta_m \approx 2\zeta_i$. In other words, the maximum complex parameter uncertainty allowed would be approximately limited to 2 times the damping ratio of the flexible modes. Note that this limitation is due to the complex nature of uncertainty allowed and is not necessarily an indication of the real parameter uncertainty that can be tolerated by the system. This may be overcome by modeling uncertainties in real parametric form and using mixed μ analysis, but, as mentioned earlier, the computation of μ is costly, making its use in the nonlinear programming optimization prohibitive. Keeping in mind that the control authority is limited around the flexible modes, such that the controller would be rolling off before the first flexible mode, a more useful criteria for robust stability under parametric uncertainty may be established. Assume that it is desired to allow for 25% uncertainty in the first two flexible modes. Note that because of the limited control authority one need not be concerned with positive variations in these modes, but rather in variations that bring the frequency of these modes closer to the bandwidth of the controller. To do this, instead of the robust stability of $H_m(jw)$, robust stability of two perturbed models of the system is considered. Denote these perturbed models by $H_m^1(jw)$ ad $H_m^2(jw)$, with $H_m^1(jw)$ and $H_m^2(jw)$ corresponding to $H_m(jw)$ with the frequencies of the first two flexible modes decreased by 10% and 25%, each. Robust stability is then implied by requiring

$$\begin{aligned} \left\|H_m^1(jw)\right\|_\infty &< \frac{1}{\delta_m^1} \\ \left\|H_m^2(jw)\right\|_\infty &< \frac{1}{\delta_m^2} \end{aligned} \tag{31}$$

These conditions are intuitively expected to provide robust stability since the control authority is low around these modes, i.e., the controller is rolling off.

Controller Design via Optimization

As mentioned previously, the parameters of the controllers are designed via nonlinear programming techniques. In this approach, the parameters of the LQG/LTR synthesis approach are chosen to optimize the pointing performance of the system while satisfying a set of H_∞–type robust stability constraints along with other constraints to impose performance specifications or cost limitations. This optimization-based approach provides a systematic means of designing optimal MIMO controllers for the attitude control of the Lewis spacecraft. Although, a mixed H_2/H_∞ synthesis is pursued here, other synthesis techniques may be easily implemented as well. Furthermore, other performance and cost specifications may be readily implemented also. The design optimization problem is formulated as follows.

Using any linear, time invariant MIMO controller, the closed-loop system dynamics can be written as

$$\dot{\bar{x}} = \bar{A}\bar{x} + \bar{L}p; \quad y_p = \bar{C}_p\bar{x}; \quad u = \bar{C}_u\bar{x} \tag{32}$$

where $\bar{x}$ is the state vector for the closed-loop dynamics, $p(t)$ is a zero mean, white noise disturbance applied at the disturbance locations, y_p is the line-of-sight pointing error, $u(t)$ is the control vector, and $\bar{A}$, $\bar{L}$, $\bar{C}_p$ and $\bar{C}_u$ are the corresponding closed-loop system matrices. The steady state covariance matrix for the closed loop state, $\Sigma_{\bar{x}}$, is computed by solving the following Lyapunov equation [5]

$$\bar{A}\Sigma_{\bar{x}} + \Sigma_{\bar{x}}\bar{A}^T + \bar{L}\Sigma_p\bar{L}^T = 0 \tag{33}$$

where Σ_p is the covariance matrix for the disturbance noise, $p(t)$. The steady-state average control power is given as

$$P = \lim_{t\to\infty} \; Tr\{E\{u(t)u^T(t)\}\} = Tr[\bar{C}_u\Sigma_{\bar{x}}\bar{C}_u^T] \tag{34}$$

and the root-mean-square line-of-sight pointing error is

$$R = \lim_{t\to\infty} \left[Tr(E\{y_p(t)y_p^T(t)\})\right]^{\frac{1}{2}} = \left[Tr(\bar{C}_p\Sigma_{\bar{x}}\bar{C}_p^T)\right]^{\frac{1}{2}} \tag{35}$$

The control design optimization problem is posed as:

$$\begin{matrix} \min \; P \\ \left\{\bar{V}, \bar{W}, \alpha, \beta, \theta\right\} \end{matrix} \tag{36}$$

s.t.

$$\begin{aligned} \|H_i(jw)\|_\infty &< \frac{1}{\delta_i} \\ \|H_o(jw)\|_\infty &< \frac{1}{\delta_o} \\ \|\delta_a(jw)H_a(jw)\|_\infty &< 1 \\ \left\|H_m^1(jw)\right\|_\infty &< \frac{1}{\delta_m^1} \\ \left\|H_m^2(jw)\right\|_\infty &< \frac{1}{\delta_m^2} \\ R(1,1) &\le e_{roll} \\ R(2,2) &\le e_{pitch} \\ R(3,3) &\le e_{yaw} \\ \sigma_i\left(\bar{C}\left(j\omega_{orb}I - \bar{A}\right)^{-1}\bar{B}\right) &\le \sigma_{orb\;;i=1,2,3} \end{aligned} \tag{37}$$

Here, The first five constraints are H_∞–norm robust stability constraints. In the next three constraints, e_{roll}, e_{pitch}, and e_{yaw} represent the desired upper bound values for the spacecraft pointing error in roll, pitch, and yaw, respectively. The last three constraints are on the singular values of the closed-loop transfer function at orbital frequency to impose disturbance rejection requirements for environmental disturbances. The variables ω_{orb} and σ_{orb} denote the orbital frequency and upper bound value for the gain, respectively. This optimization-based synthesis technique is used in the next section to design MIMO ACS for the Lewis spacecraft.

Numerical Examples

The optimization-based mixed H_2/H_∞ synthesis technique described in the previous sections has been used to design MIMO ACS controllers for the Lewis spacecraft. A number of controllers were designed for various performance and cost specifications. In this section, the design and simulation of one of these controllers are discussed. As mentioned previously, the design variables available for optimization are contained in the elements of the covariance matrices W and V, as well as the diagonal elements of matrices α, β, and θ. The process noise covariance matrix W is expressed in terms of its Cholesky decomposition, i.e.,

$$W = L_w L_w^T \tag{38}$$

where the matrix L_w is a 3 x 3 lower triangular matrix. In this control design, the six nonzero elements of L_w are used as design variables. The measurement noise covariance matrix V is assumed to be diagonal, and its three diagonal elements are used as design variables. The nine design variables associated with the covariance matrices W and V, together with the nine design variables associated with the diagonal elements of matrices α, β, and θ, constitute the 18

design variables used in the design optimization. The design optimization was performed using the Automated Design Synthesis (ADS) program. Gradient computations were performed using finite difference approximations. An interior penalty function method of ADS was used to solve the nonlinear programming problems. In this method, the constrained optimization problem is transformed into an unconstrained problem through creation of a pseudo-objective function, which is the sum of the original objective function and an imposed penalty function (a function of the constraints [6]).

The parameters associated with the optimization constraints for stability robustness, pointing accuracy, loop shaping, etc., are described in the following:

1. The scalar parameter δ_i was chosen at 0.5 to provide input uncertainty levels comparable to the baseline design.
2. The scalar parameter δ_o was chosen at 0.5 to provide output uncertainty levels comparable to the baseline design.
3. The scalar transfer function $\delta_a(jw)$, which bounds the unmodeled dynamics of the plant as well as any of its potential perturbations or uncertainty, was chosen as

$$\delta_a(jw) = \frac{-\omega^2 + 2j\omega + 1}{-\omega^2 + 100j\omega + 2500} \tag{39}$$

   This proper transfer function would bound the unmodeled dynamics of the spacecraft plant.
4. The scalar parameters δ_m^1 and δ_m^2 were chosen at 0.005 to ensure the feasibility of the constraints (for parametric uncertainty) within the design optimization.
5. The pointing accuracy threshold for roll, e_{roll} was chosen at 0.025 to provide three fold improvement over the baseline design.
6. The pointing accuracy threshold for pitch, e_{pitch} was chosen at 0.025 to provide three fold improvement over the baseline design.
7. The pointing accuracy threshold for yaw, e_{yaw} chosen at 0.035 to provide comparable pointing performance to the baseline design.
8. The required attenuation at the orbital frequency, σ_{orb} was chosen at 15 dB to provide improved orbital disturbance rejection over the baseline design.

The design optimization resulted in a 44–order controller which satisfied all design, performance and robustness constraints. Two simulations were set up using the MATLAB v4.2/SIMULINK v1.3c simulation package on a SPARCsystem 600 Sun workstation, one for the designed MIMO ACS controller and the other for the baseline SISO ACS controller. The controller block in the simulation is implemented using the MIMO subroutine, developed by NASA Langley in C programming language, with the aid of the SIMULINK user-defined S-function. Both simulations used a 28-mode state space model of the Lewis spacecraft. However, no hardware dynamics (e.g., rate gyros, reaction wheels) were included in any of the simulations. Both simulations included full models (as they were available) of reaction wheels, rate gyros, and the star tracker. A Kalman filter was designed and used to estimate the vehicle's attitude from the sensor data. The reaction wheel dynamics included friction and stiction models, limits on the input command voltages and digital voltage quantization, as well as the quantization effects on wheel RPM outputs due to the wheel's optical encoder. To each gyro dynamic model output channel, random signals were added, which represent random drift walk and instrument noise. The modeling of the star tracker included noise and alignment errors. The spacecraft was subjected to environmental disturbances, which included gravity gradient torques, drag torques, magnetic unloading, etc. Each simulation was run for one orbit, with each orbit assumed to be 5996 seconds in duration.

Figures 10–12 show the spacecraft estimated attitude time histories in roll, pitch and yaw for the two simulations. These plots show the time histories from 500 seconds onwards to allow the start-up transient dynamics to die out. Figures 10 and 11 clearly demonstrate the improvement in attitude pointing in roll and pitch, where it is observed that peak to peak attitude response is reduced by a factor of 5 or more. There is no discernible change in yaw pointing as seen from figure 12. This is because the controller was mainly designed to improve roll and pitch pointing, as they effect science data considerably more. Figures 13–15 show the complete time histories of the wheel speeds for reaction wheels 1-3 for the two simulations. It is observed from these figures that the wheel speeds for the baseline SISO and MIMO controllers are fairly close to each other, particularly in steady-state, indicating that there is little penalty (in terms of power required) that is paid by the MIMO controller for providing a better pointing performance. It is also noted from these figures that the MIMO controller has higher frequency content, which indicates the increased bandwidth of the controller.

In conclusion, the optimal mixed H_2/H_∞ controller provided substantial improvements in the pointing performance of the Lewis spacecraft over those provided by the baseline controller. This improvement was achieved while satisfying all robust stability conditions as well as other design or performance specifications. Furthermore, the power required to achieve such an improvement in pointing performance is minimal and well within the capacity of the reaction wheels in normal pointing mode. It should be noted that the proposed mixed H_2/H_∞ approach follows the conventional design approach in that it satisfies the various robust stability conditions against input, output, parametric, and nonparametric uncertainties, individually. However, if it desired to

analyze controller robustness in a collective sense, a mixed μ analysis [4] may be performed.

Concluding Remarks

The enhanced attitude control system experiment, which is a technology demonstration experiment on the NASA's small spacecraft technology initiative program's Lewis spacecraft to evaluate advanced attitude control strategies, has been described. The purpose of the experiment is to evaluate the feasibility of designing and implementing robust MIMO attitude control strategies for enhanced pointing performance of spacecraft to improve the quality of the measurements of the science instruments. Among the many control design strategies being considered for the experiment, a control synthesis technique based on mixed a H_2/H_∞ approach has been presented. The control synthesis uses a nonlinear programming technique to tune the controller parameters and impose robustness and performance constraints. Simulations were carried out to demonstrate the feasibility of the proposed attitude control design strategy, and have shown that the mixed H_2/H_∞ attitude control designs can provide substantial improvement in the pointing performance of the spacecraft over the conventional SISO designs, with minimal increase in required power, while maintaining reasonable degree of robustness against modeling and hardware uncertainties. An efficient algorithm, both in time and memory requirements, for the implementation of MIMO controllers has been developed. The algorithm has been incorporated within the on-board flight computer software.

Acknowledgment

The author would like to express his appreciation to Mr. Dean W. Sparks, for performing and providing the simulation results.

References

[1] GE Aerospace; "Pointing and Orbit Study Update (AFM T-9)" , NAS5–32500, May 22, 1992..

[2] J. R. Wertz, "Spacecraft Attitude Determination and Control," Chapter 18, Ed. by James R. Wertz, *Kluwer Academic Publishers*, Boston, MA, 1978.

[3] J. M. MacieJowski, ''Multivariable Feedback design,'' *Addison-Wesley Publishing Co.*, New York, NY, 1989.

[4] J. C. Doyle, ''Analysis of Feedback Systems with Structured Uncertainties,'' *IEEE Proc.*, Vol. 129, pt. D., No. 6, Nov. 1982, pp. 242–250.

[5] R. F. Stengel, ''Stochastic Optimal Control - Theory and Applications'' *John Wiley \& Sons, Inc.*, New York, NY, 1986.

[6] G. N. Vanderplaats, ''ADS–A Fortran Program for Automated Design Synthesis–version 1.10,'' Contractor Report 177985, NASA, 1985.

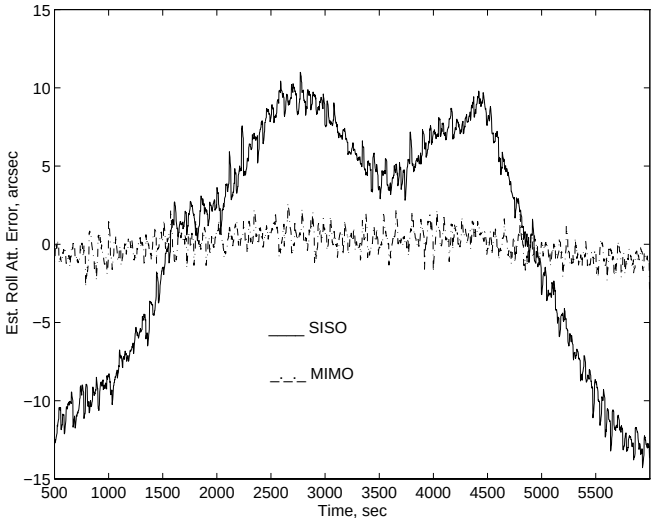

Figure 10. Time histories of estimated roll attitude for Lewis spacecraft

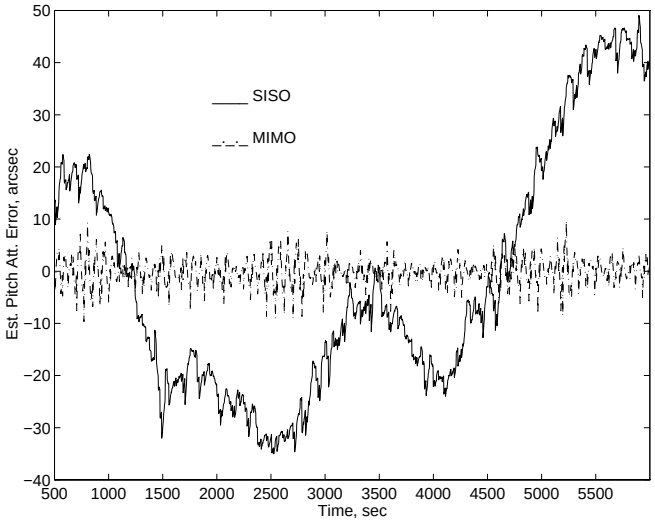

Figure 11. Time histories of estimated pitch attitude for Lewis spacecraft

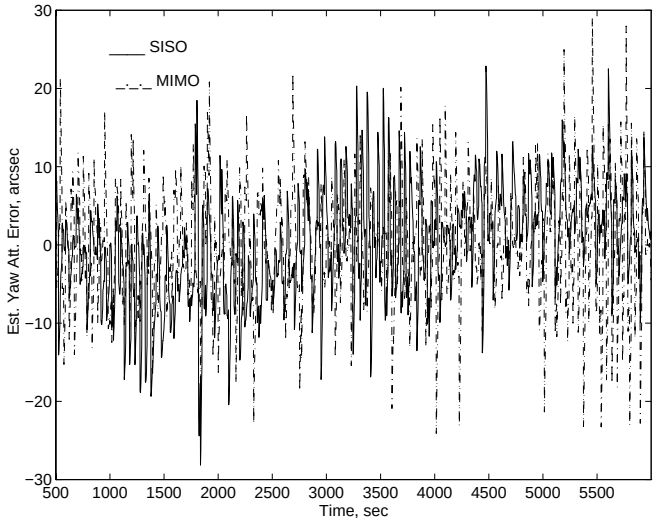

Figure 12. Time histories of estimated yaw attitude for Lewis spacecraft

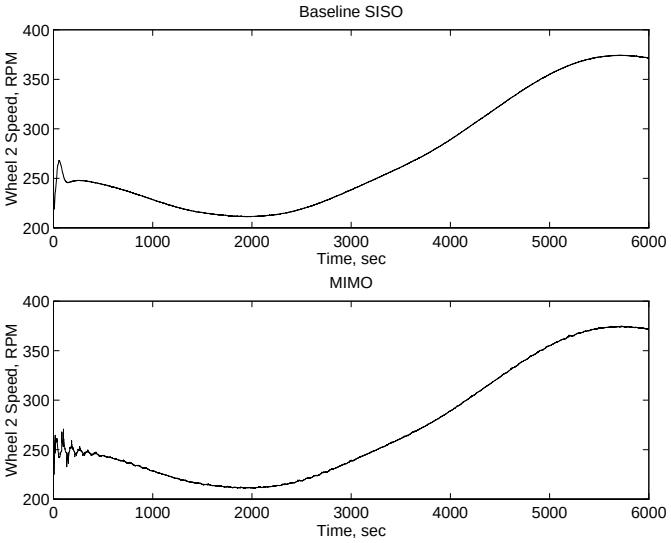

Figure 14. Time histories of the wheel speed for reaction wheel no. 2

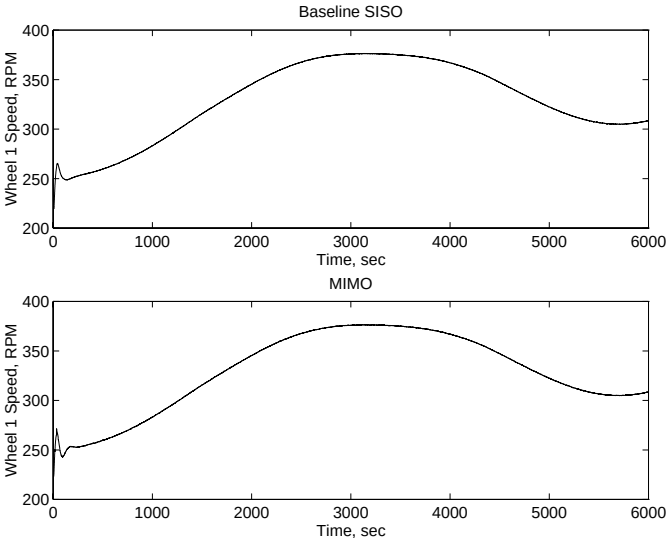

Figure 13. Time histories of the wheel speed for reaction wheel no. 1

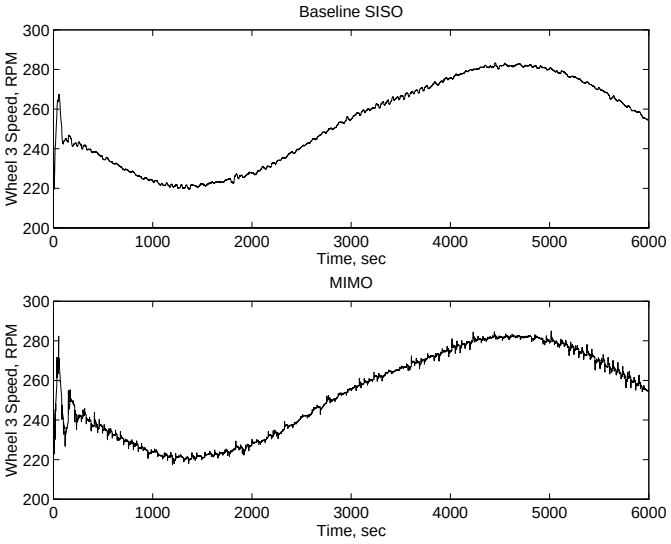

Figure 15. Time histories of the wheel speed for reaction wheel no. 3